Human Histology

A MICROFICHE ATLAS

VOLUME ONE CELLS AND TISSUES

Stanley L. Erlandsen and Jean E. Magney

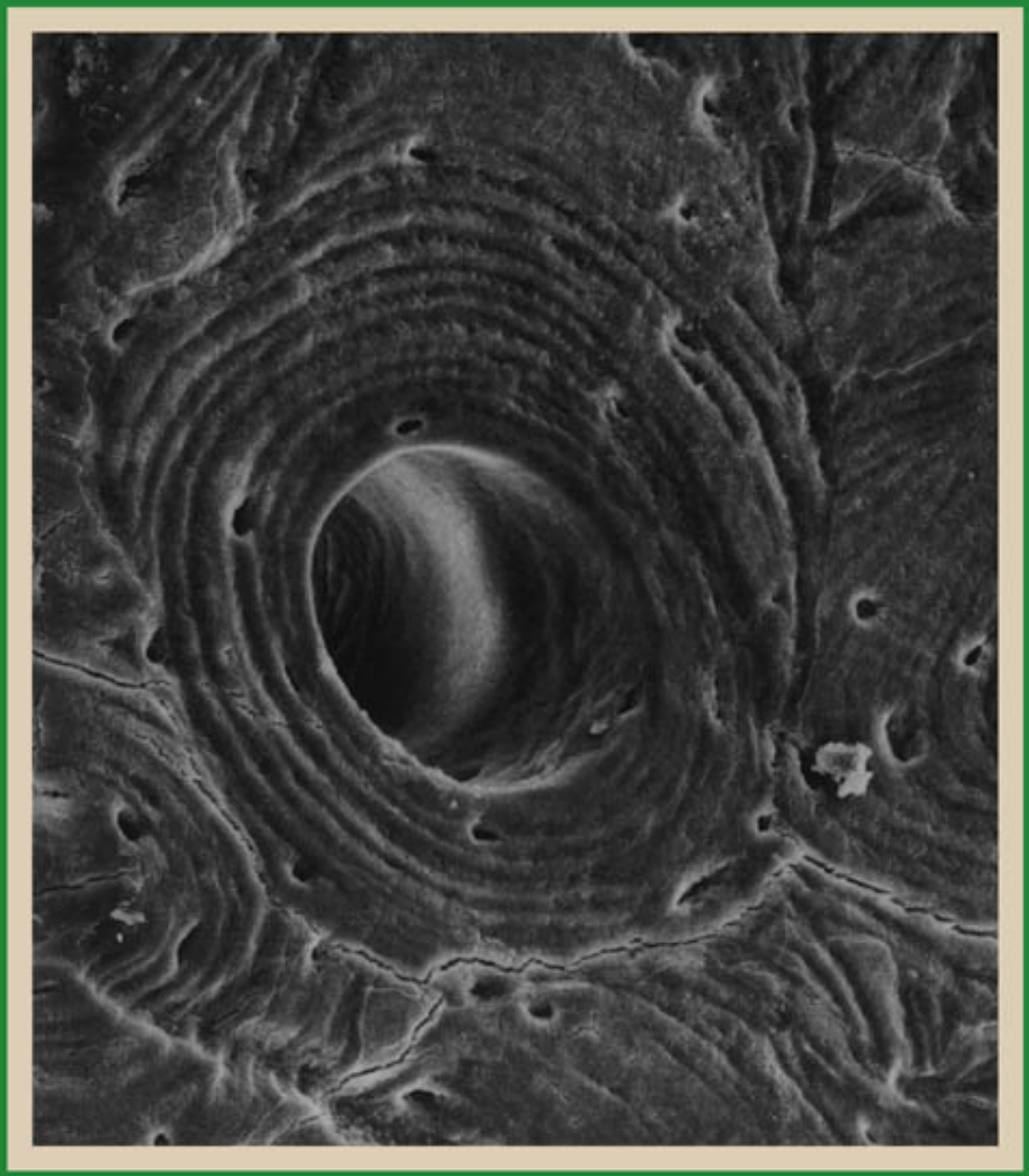

Human Histology

Volume 1

Publications in the Health Sciences

Publication of this book was assisted
by a McKnight Foundation grant to the
University of Minnesota Press's
program in the health sciences.

HUMAN HISTOLOGY
A Microfiche Atlas

Volume 1
CELLS AND TISSUES

Stanley L. Erlandsen
and Jean E. Magney

University of Minnesota Press □ Minneapolis

Published by the University of Minnesota Press.
2037 University Avenue Southeast, Minneapolis MN 55414

Published simultaneously in Canada by Fitzhenry & Whiteside Limited, Markham.

Printed in the United States of America

Library of Congress Cataloging-in-Publication Data
Erlandsen, Stanley L.
Human Histology
(Publications in the health sciences)
Includes index.
Contents: v. 1. Cells and tissues—v. 2. Organs and systems.
1. Histology—Atlases. 2. Microfiches. I. Magney, Jean E. II. Title. III. Series. [DNLM: 1. Histology—atlases. 2. Histology—Microfiche. QS 17 E69h]
QM557.E75 1985 611'.018 85-8566
ISBN 0-8166-1385-0 (set)
ISBN 0-8166-1386-9 (v. 1)
ISBN 0-8166-1387-7 (v. 2)

To our spouses,
Betty Erlandsen and Robert Magney,
for their patience, understanding,
and unswerving support.

Contents

This page intentionally left blank

Preface

This microfiche atlas of human histology is designed to help students acquire a better understanding of histology and the dynamic activities of cells, tissues, and organs. Each volume stresses the interrelationships of light microscopic and ultrastructural features and illustrates structural-functional correlations by use of schematic diagrams. In addition to our own light and electron microscopic slide collection, we have utilized more than 300 micrographs from leading scientists as well as a number of excellent macrophotographs from Lennart Nilsson and micrographs from the cinephotomicroscopy of Dr. Richard Blandau.

To use this atlas in conjunction with any histology course, the student can consult the Contents or the Index to find individual images or groups of images. We have tried to enhance the student's understanding of the material by illustrating a specific structure in a number of different ways, so that adjacent frames show it as a drawing, light micrograph, electron micrograph, and so on. Adjacent frames may also present the same structure by light microscopy at low and high magnification to help orient the student and to serve as a transition to electron microscopy.

This atlas serves as a portable visual aid for the examination of cells, tissues, and organs outside the standard laboratory setting. To facilitate its use outside the classroom, the microfiche can be examined with any portable microfiche reader that has a 15X lens. The high quality of image reproduction in the microfiche has made it a valuable aid for group study when used with a microfiche projector. The WSI Informant II microfiche projector has been successfully used in the histology labs and the Biomedical Learning Center at the University of Minnesota; it has a removable lid that permits it to be used either as a portable microfiche reader or as a microfiche projector.

Five microfiche are included in Volume 1, nine in Volume 2. Each fiche contains 63 frames identified by rows (A) and columns (1-9). The text presents captions that are keyed to the fiche: fiche number (1-14) appears as a heading, and to the left of each caption are the letter and number of the frame described (A1, A2, A3, . . .; B1, B2, B3, . . .; and so on). Unless otherwise indicated, the captions describe cells, tissues, and organs that are either of human origin or from animals whose morphological features are indistinguishable from humans. A few abbreviations are used throughout the text:

EM	Electron Micrograph
FF	Freeze Fracture
H & E	Hematoxylin and Eosin Stain
LM	Light Micrograph
SEM	Scanning Electron Micrograph
TEM	Transmission Electron Micrograph

When abbreviations appear directly on an illustration, they are explained in the accompanying caption.

A 35 mm slide set covering the same material is also available through Minnesota Histographics, 2817 Aquila Avenue North, New Hope, MN 55427.

This microfiche atlas was developed for medical students at the University of Minnesota Medical School in response to their need for

an atlas that would correlate the structural information seen by modern light and electron microscopic techniques. We would like to acknowledge the contributions made by medical students at Minnesota who so enthusiastically used and studied the microfiche and made constructive comments to help us improve the atlas. We are grateful to the Educational Development Program and the Medical School administration at the University of Minnesota for their support. Most important, we wish to thank Dr. David W. Hamilton, Head of the Department of Anatomy, for his encouragement, enthusiastic support, and generosity in helping us complete this project. Numerous individuals, including more than 150 contributors of pictures, have also helped make the microfiche a successful tool for reviewing histology. In particular, we wish to thank: Cathy Sulik for her organizational skills in maintaining the histology slide collection; Chris Frethem for his assistance in electron microscopy and photographic reproduction; Walter Gutzmer for his photographic assistance; Jennifer Steinert for her careful typing of the Index; and Dr. Anna-Mary Carpenter for her development of the excellent histology slide collection at the University of Minnesota.

Human Histology

Volume 1

This page intentionally left blank

A1 Drawing of composite, polarized epithelial cell, comparing ultrastructural components as viewed by electron microscopy (EM) and light microscopy (LM). Mitochondria are visualized at LM levels by use of special stains (in this case iron hematoxylin).

A2 Three-dimensional representation of simple columnar cells showing organelles, microvillous (striate) border, and basement membrane. The lateral borders of cells interdigitate, and junctional complexes at the apical borders join them into a tissue called epithelium.

A3 Intestinal epithelium of simple columnar cells as seen by LM. Visible also in the epithelium are mucus-secreting goblet cells, lymphocytes between the lateral borders of columnar cells, microvillous border adjacent to the lumen, and basement membrane subtended by connective tissue called the lamina propria. (H & E)

A4 Intestinal epithelium with goblet cell as seen by transmission electron micrograph (TEM). Compare with A2 and A3. Identify mucus-containing secretion granules, microvillous border, nuclei, mitochondria, lateral cell border, Golgi, and basement membrane. A wandering granulocyte (white blood cell) is seen between epithelial cells (lower right).

A5 Simple columnar epithelial cells of gallbladder as seen by scanning electron micrograph (SEM). Notice evaginations of lateral cell surfaces, which interdigitate with membranes of adjacent cells. See A4 for the appearance of these surface projections by TEM.

A6 Diagram of cell membrane (plasmalemma, unit membrane) that has been freeze-fractured (FF). Notice that the fracture plane passes through the lipid bilayer and that intramembranous particles tend to remain with the protoplasmic face (PF face). The extracellular face (EF face) is generally characterized by pits or depressions, which remain when intramembranous particles pull free as a result of the fracture. ES, extracellular surface.

A7 Comparison of TEM and FF on same cell type:
A. TEM of cell showing nucleus (N), mitochondria (M), lysosomes (L), and cell surface (plasmalemma).
B. FF of cell showing nucleus (N) with nuclear pores, lysosomes, endoplasmic reticulum (er), and protoplasmic face of cell plasmalemma (CC).

A8 FF of two adjacent cells. Extracellular space traverses from mid-left to upper right, separating particle-rich PF face of top cell from particle-poor EF face (lower left) of bottom cell. At mid-right, note approximation of both leaflets (EF and PF) of the lower cell plasmalemma as seen in cross fracture.

A9 Diagram of nucleus, nuclear envelope, and endoplasmic reticulum which is confluent with perinuclear cisterna of nuclear envelope.

B1 Liver as seen by LM. Note the large, vesicular nuclei of the hepatocytes, as well as the dark, more condensed nuclei of cells lining (or within) the vascular channels which separate hepatocytes. Compare with B2 and B3, which are at the same magnification. (H & E)

B2 LM comparing size of large motor neuron (upper center) and that of red blood cells within a capillary (lower center). Red blood cells are the only cells lacking nuclei. The nucleus of the motor neuron exhibits a large, dense nucleolus typical of protein-synthesizing cells. In keeping with this synthetic activity, the chromatin is dispersed (euchromatic), giving the nucleus a vesicular appearance. Other small, dense nuclei in the field belong to neuroglial cells. (H & E)

B3 LM of condensed nuclei of lymphocytes closely packed within a lymph node. The more vesicular nuclei of a second population of cells are interspersed with the lymphocytes, and the elongate nuclei of cells lining the blood vessel run diagonally across the right side of the field. (H & E)

B4 TEM of cell showing diaphragm-covered pores in nuclear envelope. Note the appearance of eu- and heterochromatin.

B5 FF revealing pores in an otherwise smooth nuclear envelope. Surrounding the nucleus are cytoplasmic matrix (cm) and elements of endoplasmic reticulum (er). Direction of shadow is from upper right in this FF.

B6 LM of liver stained (with toluidine blue) to show chromophil substance (ribonucleoprotein, ribosomes). Compare with B1.

B7 Chromophil substance as visualized by LM in large Purkinje cells of cerebellum. Note that nucleoli stain prominently also. They consist largely of protein and RNA, and function in the synthesis of the major components of ribosomes. (toluidine blue)

B8 Large lymphocytes in medulla of lymphatic nodule as seen by LM. These lymphocytes contain many ribosomes (chromophil substance) and are active in protein synthesis, whereas lymphocytes at periphery of nodule are relatively inactive in protein synthesis, and hence are unstained. (toluidine blue)

B9 LM of acinar cells of pancreas. These cells, which are active in the secretion of proteinaceous digestive enzymes, exhibit intense staining (with toluidine blue) for chromophil substance (ribosomes) in the basal cytoplasm. The central portion of each acinus is colorless owing to the presence of unstained secretion granules. Note unstained duct cells (left) and unstained cells in a pancreatic islet (right).

C1 Plasma cell (TEM) packed with cisternae of endoplasmic reticulum, which are dilated and filled with protein (antibody). Notice that the cisternae are studded on their outer surfaces with ribosomes, distinguishing them as rough endoplasmic reticulum (RER).

C2 TEM of connective tissue and endothelial cells containing free ribosomes scattered throughout cytoplasm, as well as sparse cisternae of smooth and rough endoplasmic reticulum.

C3 Circular profiles of smooth endoplasmic reticulum (SER) in addition to a few longitudinal profiles of rough endoplasmic reticulum as seen by TEM of a liver cell. These elements (SER) of the endoplasmic reticulum have no ribosomes attached to the cisternae and, depending on the cell type, may have diverse functions.

C4 Epithelium of epididymus stained for LM by silver impregnation method (with gold toning) to visualize Golgi apparatus, seen as black lamellae located between apex of cell and nucleus (unstained). See A1. Spermatozoa are visible in lumen.

C5 Profiles of Golgi as seen by LM in cells of pancreatic acini, lying between unstained nuclei and cell apices. Secretions of these cells are released through the apical membranes into the lumen of the acinus. See B9 for comparison. (silver impregnation and gold toning)

C6 LM of plasma cell of bone marrow exhibiting negative image (Hof) of Golgi apparatus adjacent to nucleus in eccentrically placed cytoplasm. (Wright's stain)

C7 Three-dimensional diagram of Golgi apparatus. Transfer vesicles bud off the rough endoplasmic reticulum, carrying secretory product precursors to the Golgi (forming face), where they are modified and transferred via secretory vesicles (mature face) to secretion granules or the cell surface.

C8 TEM of intestinal Paneth cell. It shows curved profiles of the saccules of the Golgi apparatus embracing a large secretory vesicle that is leaving the maturing face. Notice transfer vesicles between rough endoplasmic reticulum and the forming face of Golgi.

C9 LM illustrating double staining of Golgi apparatus. Frame A is a phase contrast micrograph of a tissue culture cell cytochemically stained for TPPase activity. The TPPase positive Golgi apparatus appears to be localized in the perinuclear region. Frame B, an immunofluorescence micrograph of the same cell, shows the localization of a 110K dalton protein in the Golgi apparatus and that the protein is coincident with the TPPase stain.

D1 Diagram of mitochondrion showing structural relationships and distribution of biochemical components.

D2 Mitochondria in liver cells stained for LM with iron hematoxylin. Amorphous shapes between liver cells (in vascular spaces) are heavily stained red blood cells.

D3 LM of mitochondria in intestinal epithelial cells. The mitochondria are seen as gray vertical rods between nucleus and the cell surface. See A1. (iron hematoxylin)

D4 Circular profiles of mitochondria with cristae in TEM of tumor cells. What other cell organelles are recognizable?

D5 Depiction of four mitochondrial types:

Upper left: inner membranes follow irregular course in formation of cristae. Gallbladder cell.

Upper right: Om, outer membrane; Im, inner membrane; M, matrix; D, dense granule. Kidney cell.

Lower left: Cr, cross-sectioned tubular cristae; Le, longitudinally sectioned tubular cristae; Cir, circularly arranged tubules. Ovarian cell.

Lower right: Le, longitudinal section; Cr, cross section. Liver cell.

D6 Diagram of mitotic cycle.

D7 Onion root tip at LM level demonstrating cells in mitosis: prophase, metaphase, and early telophase, as well as interphase cells. (iron hematoxylin)

D8 LM of onion root tip showing excellent examples of anaphase and telophase, as well as daughter cells. Note that daughter cells are distinctly smaller than interphase cells. (iron hematoxylin)

D9 LM illustrating round profiles of intestinal crypts surrounded by connective tissue. Within the central crypt, two epithelial cells have entered mitosis and are seen in metaphase-anaphase stage. These cells are easily distinguished from interphase cells (vesicular nuclei). (H & E)

E1 TEM of mitotic spindle showing chromosomes in metaphase. Electron-dense chromosomes are attached to spindle microtubules. Centrioles are seen at one pole of the spindle (upper right).

E2 Kinetochore: the constricted part of the chromosome to which spindle fibers (microtubules) attach during mitosis (see insert at right for higher magnification). TEM. C, centriole; K, kinetochore; NE, nuclear envelope.

E3 TEM of centriole with satellites which serve as nucleation sites for microtubules. Cytoplasmic filaments and polyribosomes are also visible.

E4 Immunofluorescent micrograph demonstrating localization of actin within NRK tissue culture cells. Bundles of actin filaments, sometimes called stress fibers, can be seen coursing in a diagonal pattern through the cytoplasm and around the periphery of the cell.

E5 Immunofluorescent micrograph of cytoskeletal proteins in tissue culture cells derived from bovine mammary gland. Frame a shows localization of actin; frame b, of tubulin in microtubules; frame c, localization of desmosomes by antibodies to desmosomal placque protein; and frame d, the absence of the intermediate filament protein vimentin.

E6 TEM of adluminal portions of two polarized cells. It shows the junctional complex (called a terminal bar at LM level—see G4) and the microfilaments of the terminal web just deep to the microvillous border. Note also desmosome with tonofilaments extending into cytoplasm of each cell. Lateral borders of cells interdigitate.

E7 Polarized epithelial cells of intestinal crypts (TEM) exhibiting a variety of secretion granules. Paneth cells (center), with large circular secretion granules, will release their secretory product by exocytosis into the crypt lumen (top). The endocrine cell (lower right), with small granules, is oriented basally, rather than adluminally, and will discharge its product into capillaries instead of the lumen.

E8 Diagram of eight subdivisions of epithelia. Epithelium is a tissue that covers free surfaces of the body. The cells are contiguous and rest upon a basement membrane.

E9 LM showing simple squamous epithelium lining Bowman's space of renal corpuscle and simple cuboidal epithelium forming distal convoluted tubule of kidney. (H & E)

F1 Simple squamous cell of mesothelium in TEM of visceral peritoneum of intestine. Beneath the basement membrane, elements of connective tissue and smooth muscle cells are present.

F2 Simple cuboidal epithelium of pancreatic duct by LM. The duct is surrounded by connective tissue and pancreatic acini. (H & E)

F3 Cross section of pancreatic duct by TEM, demonstrating simple cuboidal epithelium.

F4 LM showing simple columnar epithelium with goblet cells in small intestine. Mucus granules in goblet cells are unstained owing to the method used to fix the tissue. Intraepithelial lymphocytes are also present. (H & E)

F5 LM of pseudostratified columnar epithelium with cilia and goblet cells (respiratory epithelium). (H & E)

F6 LM of stratified squamous keratinized epithelium found in thin skin. Acidophilic connective tissue underlies the epithelium, whereas basophilic squames of dead keratinized epithelial cells border the free surface. (H & E)

F7 Stratified squamous nonkeratinized epithelium of esophagus as seen by LM. Note lack of keratinized squames on luminal surface. (H & E)

F8 LM of duct lined by stratified cuboidal epithelium. Small lymphocytes are present in the epithelium and adjacent connective tissue. (H & E)

F9 LM of duct lined by stratified columnar epithelium. Precipitated secretory product is present in the lumen, and red blood cells are present in vessels in the connective tissue. (H & E)

G1 Transitional epithelium of urinary bladder as seen by LM. Note umbrella cells (at lumen), which will stretch and flatten as the bladder fills. Capillaries with red blood cells are separated from epithelium by basement membranes of both endothelial and epithelial cells. (H & E)

G2 Diagram illustrating variety of surface specializations found in epithelial cells.

G3 Diagram of various types of junctional fine structure. These types of cell junctions allow for tight to moderate intercellular adhesion, or for communication between adjacent epithelial cells.

G4 LM of terminal bars, junctional complexes that prevent luminal contents from penetrating lateral intercellular space. These are seen here as darkly stained spots at lateral cell membranes right below the microvillous border. (H & E)

G5 TEM of terminal bar. It is made up of a zonula occludens (reduced intercellular space and punctate membrane fusion) and a zonula adherens (slightly increased intercellular space and microfilaments of the terminal web associated with a moderate density of cytoplasm). A desmosome (macula adherens), which functions in intercelluar adhesion, is also seen below this junctional complex. Microvilli containing actin filaments appear at the top of this frame. See G3.

G6 Zonula occludens (tight junction) as seen by FF. It appears as an anastomosing web (representing membrane fusion) that encircles the luminal end of the lateral membranes of each cell, attaching it to adjacent cells and sealing off the lumen from the interstitium. In the protoplasmic fracture face, the web appears as protruding ridges (composed of intramembranous particles), whereas the extracellular fracture face shows the presence of the web as linear depressions. See G2-G4.

G7 Cells of stratified squamous epithelium of skin by LM. These cells possess spiny borders, which, by TEM, are seen to be points of intercellular adhesion called desmosomes. However, the impression gained by LM resulted in the name "stratum spinosum" for this layer of the skin. (H & E)

G8 Desmosomes, as viewed by TEM (left), showing tonofilaments embedded in electron-dense plaque at junction, and extending into cytoplasm. Tonofilaments do not cross intercellular space, although recent studies suggest that some intramembranous particles in desmosomes may do so. FF (right) with etching shows irregular cytoplasmic tonofilaments related to desmosome (membrane fractured at lower left). See G3.

G9 FF revealing tonofilaments in cross fracture of cytoplasm (bottom) and aggregation of large membrane particles in extracellular fracture face of plasmalemma (top), at hemidesmosomes.

Acknowledgments

A2, D6 Reproduced with permission from *Gray's Anatomy*, 35th British edition, R. Warwick and P. L. Williams, editors, Longman, Edinburgh, Scotland, 1973.

A7 Reproduced with permission from W. T. Daems and P. Brederoo, *Mononuclear Phagocytes*, R. van Furth, editor, Blackwell Scientific Publications, Oxford, England, 1970.

A8 Courtesy of Dr. Ross Johnson, Department of Genetics and Cell Biology, University of Minnesota, Minneapolis, MN.

B4, C3 Courtesy of Dr. Paul C. Letourneau, Department of Anatomy, Medical School, University of Minnesota, Minneapolis, MN.

B5 Courtesy of Dr. Daniel Branton, Biology Laboratory, Harvard University, Cambridge, MA.

C7 Reproduced with permission from C. P. Leblond, *Histology*, 8th edition, A. W. Ham and D. W. Cormack, editors, Lippincott, Philadelphia, PA, 1979.

C9 Reproduced with permission from Jim Jung-Ching Lin and Sharon A. Orieally, Journal of Cell Biology 92:108, January 1982.

D5 Reproduced with permission from J. A. G. Rhodin, *Atlas of Ultrastructure*, Saunders, Philadelphia, PA, 1963.

E1 Reproduced with permission from B. R. Brinkley, *Bailey's Textbook of Histology*, 17th edition, W. M. Copenhaver, D. E. Kelly, and R. L. Wood, editors, Williams and Wilkins, Baltimore, MD, 1978.

E2 Reproduced with permission from B. R. Brinkley, *Advances in Cell Biology*, Vol. 1, D. Prescott, editor, Plenum Press, New York, NY, 1969.

E3 Courtesy of Ms. Gwen Crabbe, Department of Laboratory Medicine and Pathology, University of Minnesota, Minneapolis, MN.

E4 Courtesy of Dr. Judith Schollmeyer, Roman Hruska USDA Meat Animal Research Laboratory, Clay Center, NE.

E5 Reproduced with permission from Erika Schmid et al., Journal of Cell Biology 96:37-50, January 1983.

E6, G5 Courtesy of Dr. David G. Chase, Cell Biology Research Laboratory, Veteran's Administration Hospital, Sepulveda, CA.

F3 Courtesy of Dr. Jeanette Lopez-Lewellyn, Wayne State Medical School, Detroit, MI.

G6 Reproduced with permission from Adolfo Martinez-Palomo, *Electron Microscopy*, 1978, Ninth International Congress on Electron Microscopy, Vol. 3, Microscopical Society of Canada, Toronto, Canada, 1978.

G8, G9 Reproduced with permission from Douglas E. Kelly, *Bailey's Textbook of Histology*, 17th edition, W. M. Copenhaver, D. E. Kelly, and R. L. Wood, editors, Williams and Wilkins, Baltimore, MD, 1978.

A1 Diagram of freeze fracture plane passing from plasma membrane of Cell B to that of Cell A. Note that the fracture plane occurs within the lipid bilayer of each cell membrane. Intramembranous particles are usually more numerous in the protoplasmic fracture membrane face and often are seen as linear arrays in tight junctions or in gap junctions as groupings of hexagonally packed intramembranous particles. A central channel in opposing intramembranous particles (connexons) in gap junction is thought to control transport of ions and small molecules between adjacent coupled cells.

A2 Gap junction, as viewed by TEM, showing standard thin section (left) and section treated with lanthanum (right) in extracellular space to illustrate outline of particles connecting the cells.

A3 FF of gap junction between two tumor cells. Note presence of both protoplasmic face and extracellular face and appearance of gap junctions in both. See A2.

A4 LM of simple columnar epithelium of gallbladder. Compare lateral border of these columnar cells with that seen in A5 and A6. (H & E)

A5 SEM of epithelium of gallbladder showing lateral surface interdigitations.

A6 TEM of lateral surface interdigitations of basal region of two intestinal epithelial cells. A capillary with red blood cell and platelet is located immediately beneath the basement membrane.

A7 LM of pseudostratified columnar epithelium with cilia and goblet cells. The thick basement membrane (broad, smooth, and pink) lies immediately beneath the epithelium. (H & E)

A8 LM of intestinal epithelium. The periodic acid-Schiff (PAS) stain reveals carbohydrate moieties in the basement membrane, which is seen as a thin, pink line beneath epithelial cells. Glycoprotein in mucus within goblet cell and on microvillous border is also PAS-positive. (PAS stain)

A9 TEM of basement membrane of intestinal epithelium. Locate basal lamina and reticular lamina components of basement membrane. See Fiche 1, Frame A1.

B1 Drawing of surface specializations involved with amplification of luminal cell surface (microvilli) and motility (cilia). Beat of cilia is illustrated. Filamentous cores of microvilli and basal bodies of cilia are anchored in terminal web. What is the structural basis for microvilli versus cilia?

B2 LM of intestinal epithelium demonstrating striate (microvillous) border adjacent to lumen. (H & E)

B3 TEM of microvillous border of intestinal epithelial cells. Several bacteria are attached to the glycocalyx, or "fuzzy coat," of microvillous border.

B4 TEM of terminal web region of microvillous border. Bundles of microfilaments (actin) in the core of the microvillus are inserted into a network of intermediate filaments in the terminal web. Inset (lower left) shows tightly packed bundles of actin filaments in microvillous core, which are enmeshed by a fine network of cross-linked filaments.

B5 Microvillous border as seen by SEM (above) and FF (below). Note uniformity of appearance.

B6 LM of pseudostratified columnar epithelium with goblet cells and cilia. Basal bodies of cilia appear as a thin red line in the apical cytoplasm. (H & E)

B7 TEM of ciliated pseudostratified columnar epithelium in middle ear mucosa. Note cilia and microvilli on apical surfaces of the cells. Compare with B8.

B8 SEM of cilia and microvilli on same cell (low magnification, left; high magnification, right) in pseudostratified columnar epithelial cells of bronchial mucosa. Compare the dimensions of cilia with those of microvilli.

B9 SEM of cilia and microvilli on luminal surface of rat trachea. Notice that apical surfaces of cells are distinct from one another and that in some cells cilia predominate whereas in others microvilli do.

C1 Diagram of pathways of lysosomal system involved with intracellular digestion and endocytic uptake. Review the role of the Golgi apparatus in lysosome formation.

C2 LM showing lipofuscin pigment (residual bodies) in liver cells as gold-brown granules. (H & E)

C3 TEM of autophagic vacuoles in cytoplasm of intestinal epithelial cells. Examples of cell organelles can be seen within vacuoles.

C4 TEM of intestinal Paneth cell demonstrating residual body (left) and phagosome (right) containing intestinal microbe with serrated border. A portion of the Golgi apparatus can be seen beneath these lysosomal elements.

C5 LM of mesenchymal cells of pig embryo. These cells are precursors of a variety of cells of connective tissue. (H & E)

C6 Reticular cell (center) with large vesicular nucleus, seen by LM within a lymph node where it produces reticular fibers of the stroma (framework) of this organ. (H & E)

C7 LM of fibroblasts (center). They produce precursors of extracellular fibers of connective tissue: collagen, elastin, and reticular fibers. (H & E)

C8 TEM showing elongate, spindle shape of fibroblast and, in contrast, rounded plasma cell below it. What type of tissue is seen at top?

C9 LM of adipocyte. The nucleus is eccentrically placed in an attenuated cytoplasm which surrounds lipid inclusion. (H & E)

D1 TEM of adipocyte from subcutaneous tissue of six-month-old fetus. The nucleus (N) is pressed to one side of the cell by the large lipid droplet (Ld). The cytoplasm is reduced to a thin rim containing small Golgi complexes and mitochondria. Collagen fibers (Cf) and fibroblasts (Fb) are seen at left.

D2 Blank

D3 SEM of cluster of adipocytes. Fibrous strands represent part of the supportive reticular network.

D4 LM of macrophage in whole mount of mesentery. Cytoplasm contains vacuoles of irregular size. (iron hematoxylin stain)

D5 LM of free macrophage in loose connective tissue. Note the presence of irregular cytoplasmic vacuoles. (H & E)

D6 Free macrophage (TEM) exhibiting numerous cytoplasmic infoldings, vacuoles, coated vesicles, and residual bodies. Examples of collagen fibers and unmyelinated nerve fibers are also seen.

D7 SEM of mouse macrophage ingesting opsonized red blood cells.

D8 LM of fixed macrophages (Kupffer cells) containing trypan blue lining sinusoids of liver. Trypan blue dye, injected intravenously, was taken up by these macrophages by phagocytosis. (H & E)

D9 Fixed macrophage (center) in lymph node exhibiting frothy, vacuolated cytoplasm (LM). (azan stain)

E1 LM of perivascular location of mast cell (center) in whole mount of mesentery. (toluidine blue stain)

E2 LM of mast cells in connective tissue. Notice large, densely packed granules and central nucleus. (aldehyde fuchsin stain)

E3 TEM of mast cell. Granules contain histamine, which increases permeability of small venules and produces edema, and heparin, an anticoagulant. A portion of a capillary is seen (left and bottom).

E4 TEM of mast cells from lung before and after stimulation. Compare unstimulated cell (left) with the cell exposed for five minutes to anti-IgE antibody (right), which triggered the mast cell to discharge its secretory granules. The massive secretory response by the mast cell produces secretory channels in the cytoplasm that are continuous with the extracellular space. Surface folds (f) are longer after stimulation. Areas free of surface fold are indicated by small arrowhead, endocytosed folds by the large arrowhead in left figure. c, crystalline scroll-like granule; a, amorphous granule; a_1-a_3 (right), granules soon to be discharged; v, vacuoles (remnants of secretory granule membrane) connected to extracellular space; n, nucleus. Secretion site is indicated by the large arrowhead at right.

E5 LM of lymphocyte in peripheral blood. Compare with red blood cells and platelets in field. (Wright's stain)

E6 LM of lymphocytes (small, dense nuclei between epithelial cells) in mucosa of esophagus. (H & E)

E7 TEM of lymphocyte. Note paucity of membranous organelles and abundance of free ribosomes in thin cytoplasmic rim. A pair of centrioles and several mitochondria are seen.

E8 LM of plasma cell in bone marrow. Nucleus is in typically eccentric position. Hof, or Golgi region, is negatively stained. (Wright's stain)

E9 LM of plasma cells with eccentric nuclei. These cells contain nuclei with "clock-face" configuration of condensed chromatin and basophilic cytoplasm. By LM, plasma cells are often seen beneath mucosal surfaces (shown here in the intestine) and in lymphoid tissue. (H & E)

F1 Plasma cell (TEM) exhibiting dilated cisternae of rough endoplasmic reticulum. This cell is active in secretion of protein (antibody). Patterns of eu- and heterochromatin are evident.

F2 LM comparison of monocyte (right), lymphocyte (left), and red blood cells (scattered throughout). The monocyte is a large cell with gray, vacuolated cytoplasm, a sprinkling of granules called azure dust, and an indented nucleus that has a "raked" appearance. The lymphocyte is smaller, with a thin rim of light-blue cytoplasm and a condensed nucleus. (Wright's stain)

F3 Monocyte (TEM) exhibiting small lysosomal granules (azure dust) and indented nucleus. Monocytes are apparent precursors of tissue macrophages.

F4 LM of polymorphonuclear leukocyte (also known as PMN, or neutrophil) in peripheral blood. Note multilobed nucleus, azure and specific granules. Compare size with red blood cells. (Wright's stain)

F5 Two polymorphonuclear leukocytes, recognizable by multilobed nuclei, seen by LM in vessel at center of field. Find plasma cells in connective tissue. (H & E)

F6 TEM of polymorphonuclear leukocyte. Note multilobed nucleus and specific granulation.

F7 LM of eosinophil in peripheral blood. Granules are large and orange, and the nucleus is often bilobed. (Wright's stain)

F8 LM of eosinophils in tissue. These stand out because of large, round, orange granules and bilobed nuclei. (H & E)

F9 TEM of eosinophil. Granules are large, membrane-bound, electron-dense, and usually contain an angular, very dense crystalloid. Nucleus is bilobed.

G1 LM of basophil in peripheral blood. Cytoplasm of mature basophil is clear and contains numerous large basophilic granules which usually overlie the nucleus. (Wright's stain)

G2 Basophil (TEM). Granules are large, regular in size and shape, and contain histamine, heparin, SRS (slow reacting substance), and serotonin, which are powerful vasoactive mediators. The granules are often disrupted owing to difficulty in fixing the tissue.

G3 Erythrocytes and platelet (TEM). Locate cisternae of dense tubular system, dense granules, and microtubules. See E5 for platelets as seen by LM.

G4 Diagram illustrating composition of ground substance in extracellular matrix. Considerable heterogeneity in proteoglycan size and structure exists between different tissues owing to variations in the number, size, or degree of sulfation of GAG chains. The proteoglycan aggregate illustrated in this frame is from cartilage. Recently fibronectin, chondronectin, and laminin (all glycoproteins) have been identified as structural elements of the connective tissue matrix. Fibronectin is a major surface glycoprotein of the fibroblast, but may be produced by other mesenchymally derived cells, by epithelial and endothelial cells, and by some marrow-cell types. It also is found in plasma and is sometimes called cold-insoluble globulin. Laminin is a constituent of basement membranes, whereas chondronectin is found within the matrix of cartilage.

G5 TEM of mast cell in connective tissue. Note the presence and size of proteoglycans (drawn in ink) in the extracellular space. Examples of collagen fibrils and fibers can also be seen in the extracellular space.

G6 Chart showing types and distribution of different collagen molecules.

G7 Drawing of fibroblast illustrating steps in intracellular synthesis and extracellular formation of collagen.

G8 LM longitudinal section of tendon demonstrating dense array of collagen fibers and interspersed fibroblasts. (H & E)

G9 TEM of fibroblasts and collagen. Note size and plane of section of collagen fibers.

Acknowledgments

A2 Courtesy of Dr. Ross Johnson, Department of Genetics and Cell Biology, University of Minnesota, Minneapolis, MN.

A3 Courtesy of Dr. Judson Sheridan, Department of Anatomy, Medical School, University of Minnesota, Minneapolis, MN.

A8, C4 Courtesy of Dr. Jeanette Lopez-Lewellyn, Wayne State Medical School, Detroit, MI.

B4 Reproduced with permission from Nobutaka Hirokawa et al., Journal of Cell Biology 94:425-43, August 1982.

B7 Courtesy of Mr. David Muchow, Department of Anatomy, Medical School, University of Minnesota, Minneapolis, MN.

C8, E3, F9, G3 Courtesy of Dr. David G. Chase, Cell Biology Research Laboratory, Veteran's Administration Hospital, Sepulveda, CA.

D1 Reproduced with permission from Tatsuo Ebe and S. Kobayashi, *Fine Structure of Human Cells and Tissues*, T. Ebe and S. Kobayashi, editors, Igaku-Shoin, Tokyo, Japan, 1972.

D7 Reproduced with permission from J-P. Revel, M. Rabinovitch, and M. J. DeStefano, *Histology*, 4th edition, L. Weiss and R. O. Greep, editors, McGraw-Hill, New York, NY, 1977.

E4 Courtesy of Dr. John Caulfield, Room 517 Seeley G. Mudd Building, Boston, MA.

E7, F6, G2 Courtesy of Dr. Janet Parkin, Department of Laboratory Medicine and Pathology, University of Minnesota, Minneapolis, MN.

F3 Reproduced with permission from J. C. Cawley and F. G. J. Hayhoe, *Ultrastructure of Haemic Cells*, Saunders, London, England, 1973.

G4 The electron micrograph is reproduced with permission from Gretchen Hascall and Vincent Hascall, *Cell Biology of Extracellular Matrix*, Elizabeth D. Day, editor, Plenum Press, New York, NY, 1981. The drawing of the model for fibronectin is redrawn and appears courtesy of Dr. Kenneth Yamada, Chief, Membrane Biochemistry Section, Department of Health, Education, and Welfare, National Institutes of Health, Bethesda, MD.

G9 Courtesy of Dr. Jerry A. Maynard, Department of Orthopedic Surgery, Carver Pavillion, College of Medicine, University of Iowa, Iowa City, IA.

A1 LM section of lymph node stained with H & E. The lymph node is an organ composed mainly of lymphocytes, which make up the parenchyma or functional part of the organ, suspended in a net or framework of reticular fibers called the stroma. Reticular fibers are colorless in this section and, therefore, are not seen.

A2 LM of lymph node permitting visualization of reticular fibers of stroma within the organ. Note arrangement of reticular fibers around small blood vessels. (silver stain)

A3 TEM of extracellular matrix subtending epithelial cell and basal lamina. Reticular fibers are generally smaller in diameter than collagen fibers, but otherwise similar, including 64-67 nm periodicity. Observe reticular fibers identified in longitudinal section as being adjacent to basal lamina and compare them with cross section of larger collagen fibers seen in bundles below. In addition, note basal lamina of epithelial cell (upper left) which is also composed of collagen (type 4). See Fiche 2, Frame G4.

A4 LM of muscular arteries. These have an internal elastic lamina that is hyaline, i.e., glassy or translucent in appearance, and that is made up of elastic fibers produced by fibroblasts and smooth muscle cells. The lamina is located near the lumen, which in fixed tissue has a folded, ribbonlike configuration. (H & E)

A5 LM of muscular artery with internal elastic lamina which is selectively stained black and which appears as folded ribbon near lumen. Compare with A4. (Verhoeff stain)

A6 Two constituents of elastic fibers: amorphous-appearing elastin and distinct microfibrils. Elastic fibers are seen in alternating layers in this TEM.

A7 Higher-magnification TEM showing microfibrillar component of elastic fibers and their arrangement around amorphous elastin (nonstaining in this fixation) more clearly than in A6. Collagen fibers are also seen.

A8 *through B7 depict types of connective tissue by LM.* Note relative abundance of cells and fibers and their arrangement. All except A9 are at the same magnification.

A8 Loose connective tissue. (H & E)

A9 Loose connective tissue, high magnification of A8. (H & E)

B1 Adipose connective tissue. (H & E)

B2 Tendon: dense, regular connective tissue. (H & E)

B3 Dermis of skin: dense, irregular connective tissue (H & E)

B4 Ligamentum nuchae: dense, regular connective tissue with compact masses of elastic fibers. (H & E)

B5 Ligamentum nuchae: dense, regular connective tissue with compact masses of elastic fibers. (Verhoeff stain)

B6 Lymph node. (H & E)

B7 Lymph node: the stroma consists of reticular connective tissue, which is made visible by use of silver stain.

B8 Diagram of chondrogenesis in cartilage. Cartilage matrix contains type II collagen, whereas types I and III may be present in perichondrium.

B9 LM of tracheal cartilage. Note that perichondrium is eosinophilic, whereas matrix of cartilage is basophilic. Respiratory epithelium is seen at upper edge of section. (H & E)

C1 SEM of tracheal cartilage similar to B9. Notice cell nests, perichondrium, and epithelium.

C2 LM of perichondrium of hyaline cartilage at higher magnification. (H & E)

C3 Isogenous cell nests in hyaline cartilage as seen by LM. Because of fixation, cell bodies have shrunk away from sides of lacunae. (H & E)

C4 SEM of cell nest in hyaline cartilage fixed by aldehyde. Chondrocytes occupy entire lacuna and are covered by short microvilli. Matrix is made of thin collagen fibrils.

C5 Chondrocyte in lacuna (TEM). Numerous microvilli are seen. Compare matrix with C4.

C6 LM of elastic cartilage in epiglottis. Elastic fibers, unstained (or light pink in older specimens), weave between lacunae. Perichondrium is at top. (H & E)

C7 LM of elastic cartilage in epiglottis. Elastic fibers are selectively stained black. (Verhoeff stain)

C8 LM of elastic cartilage and perichondrium, high magnification. (Verhoeff stain)

C9 LM of fibrocartilage. Note shape of cells, their relative numbers, and presence of fiber bundles. (H & E)

D1 LM of fibrocartilage, high magnification. Cell nests and their territorial matrix are seen in tendonlike connective tissue. (H & E)

D2 TEM of fibrocartilage. Note presence of collagen fibrils in matrix. Compare with C5. ER, endoplasmic reticulum; arrow, site of secretion; Mv, matrix vesicles.

D3 Macrophotograph of head of humerus showing spongy (cancellous) and compact bone.

D4 Drawing of microstructure of mature bone in both transverse section (top) and longitudinal section. Areas of compact and cancellous bone are included. The central area in transverse section simulates a microradiograph, the densities reflecting variations in mineralization. Note the general construction of the osteons, the distribution of the osteocyte lacunae, the Haversian canals and their contents, resorption spaces, and the different views of the structural basis of bone lamellation.

D5 SEM of cancellous bone with trabeculae (upper left) and adjoining compact bone (lower right).

D6 Drawing of osteons illustrating formation of Haversian systems and canaliculi.

D7 LM of osteon in cross section. (H & E)

D8 LM of osteon in cross section. (ground bone)

D9 SEM of osteon in cross section.

E1 Ground bone at LM level showing Haversian systems, Volkman's canals, and osteocytes in lacunae.

E2 LM of osteocytes in lacunae, connected through canaliculi. (ground bone)

E3 High-magnification LM of Haversian canal in longitudinal section (top) showing openings of canaliculi. Osteocytes in lacunae (below) receive metabolites by way of vessel in Haversian canal and by both diffusion and intracellular coupling through canaliculi. (ground bone)

E4 SEM of osteocyte in lacuna extending cytoplasmic process into canaliculus below. Observe unmineralized collagen (osteoid) surrounding cell body.

E5 TEM of osteocyte in lacuna. Processes of cytoplasm extend toward opening of canaliculus.

E6 LM of compact bone (center) exhibiting osteocytes in lacunae. On the left of the bone are osteoblasts (elongate basophilic cells), involved in the secretion of bone matrix. Note periosteum (right). (H & E)

E7 LM of columnarlike osteoblasts in pig embryo, arrayed on bone spicule during intramembranous bone formation. The osteoblasts are very basophilic because of production and secretion of protein (collagen, etc.). Osteoid appears as lightly stained areas beneath osteoblasts. (H & E)

E8 Bone formation by osteoblast (TEM). Note unmineralized periosteum (upper left). Electron-dense bone matrix (mineralized) surrounds cytoplasmic extensions into canaliculi.

E9 Blank

F1 Multinucleated, eosinophilic osteoclasts as seen by LM. One osteoclast (lower center) is in a Howships lacuna, a cavity or depression in the bone caused by the cell's action in resorbing bone matrix. (H & E)

F2 TEM of osteoclast. Notice numerous mitochondria and nuclei. Bone matrix is seen at upper left.

F3 TEM of osteoclast ruffled border in contact with bone which it is resorbing (left). Note collagen fibers in bone matrix.

F4 Diagram of differentiation of osteocytes during intramembranous bone formation.

F5 LM of intramembranous bone formation in pig embryo. Forming nasal cartilage is visible (left). See higher-magnification E7. (H & E)

F6 LM of intramembranous bone formation in flat bone of skull. Osteoblasts are lined up on surface of forming bone. Their continuous production of lamellae form Haversian systems. Early formation of diploe can be seen at this stage. (H & E)

F7 Drawing of endochondral bone formation. Pale blue cartilage model (A) develops a periosteal bone (black) collar (B) before calcification of cartilage (purple) occurs (C). Vascular mesenchyme enters the calcified cartilage and establishes the primary center of ossification (D), which then divides into two zones, one at either end of the diaphysis (E). Blood vessels and mesenchyme enter epiphyseal cartilage to establish secondary centers of ossification (F, G, H). As bone ceases to grow in length, the epiphyseal plates disappear (I, J), and the bone marrow cavity becomes continuous throughout the length of the bone. A, B, C, and D are cross sections through the centers of A, B, C, and D.

F8 Macrophotograph showing surface and cut view of tibia. Visible are compact and cancellous bone, epiphysis, and diaphysis.

F9 Diagram illustrating surfaces where bone is deposited or resorbed during remodeling at ends of growing long bones with flared extremities.

G1 LM showing (top to bottom) epiphysis, epiphyseal plate, and metaphysis of long bone. (H & E)

G2 LM of epiphyseal plate. Resting cartilage (top) and marrow cavity (bottom). (H & E)

G3 LM of epiphyseal plate at higher magnification. Note hyaline cartilage and chondrocytes in lacunae (top), and trabeculae of calcified cartilage and forming bone (bottom). (H & E)

G4 SEM of epiphyseal plate. Compare with G3.

G5 SEM of cartilage of epiphyseal plate, showing zones of proliferation, hypertrophy, and calcification.

G6 TEM of hypertrophied chondrocytes in epiphyseal plate. Note deposits of hydroxyapatite crystals (arrows) at periphery of lacunae which contain remnants of degenerating chondrocytes.

G7 LM of epiphyseal plate at high magnification. Hypertrophied chondrocytes have died, and invading vascular buds have opened lacunae in the calcified cartilage leaving spicules of cartilage on which bone is deposited by osteoblasts. Remodeling of bone/cartilage matrix by osteoclasts is an active process in this region. (H & E)

G8 SEM of epiphyseal plate showing zone of calcification and adjacent marrow, below. Compare with G5.

G9 TEM of zone of calcification in epiphyseal plate. After chondrocytes die as a result of changes in matrix, capillaries in vicinity of calcified lacunae assist in breakdown of crosswalls, thus allowing osteogenic cells to migrate in and begin deposition of new bone. W, lacuna crosswall decalcified; P, osteoprogenitor cell; M, monocytes.

Acknowledgments

A6, A7 Courtesy of Dr. Daniel H. Bodley, Department of Anatomy, Chicago College of Osteopathic Medicine, Chicago, IL.

C5, E5, E8, F2, F3 Courtesy of Dr. Jerry A. Maynard, Department of Orthopedic Surgery, Carver Pavillion, College of Medicine, University of Iowa, Iowa City, IA.

D2 Reproduced with permission from Marie Yamada, Archivum Histologicum Japonicum 39:347, 1976.

D3, F7 Reproduced with permission from Donald W. Fawcett, *A Textbook of Histology*, 10th edition, W. Bloom and D. W. Fawcett, Saunders, Philadelphia, PA, 1975.

D4 Reproduced with permission from Gray's *Anatomy*, 35th British edition, R. Warwick and P. L. Williams, Longman, Edinburgh, Scotland, 1973.

D6 Reproduced with permission from C. P. Leblond, *Histology*, 8th edition, A. W. Ham and D. H. Cormack, Lippincott, Philadelphia, PA, 1979.

F5, F6 Courtesy of Dr. P. K. Dixit, Department of Anatomy, Medical School, University of Minnesota, Minneapolis, MN.

F9 Reproduced with permission from A. W. Ham, Journal of Bone and Joint Surgery 34A:701, 1952.

G6 Courtesy of Dr. Robert Schenk, Institute of Anatomy, University of Bern, Bern, Switzerland.

G9 Reproduced with permission from Robert Schenk, Journal of Cell Biology 34:279, 1967.

A1 Drawing of longitudinal and cross sections of muscle cells, with approximate size comparisons.

A2 LM of cross and longitudinal sections of smooth muscle in wall of a small muscular artery. (H & E)

A3 Cross section of smooth muscle (TEM). Note that plane of section may not include the nucleus in all cells. The Golgi apparatus is located at pole of nucleus. See A1.

A4 TEM showing longitudinal section of smooth muscle cell in lamina propria of intestinal villus.

A5 TEM of cross sections of smooth muscle. A gap junction (nexus) joining adjacent smooth muscle cells (center) and a capillary and red blood cell (upper right) are seen. An external lamina is visible on surface of smooth muscle cells.

A6 *In vitro* contraction of smooth muscle as seen by LM cinematography and SEM.

A7 Unmyelinated nerve in bundle of smooth muscle fibers (TEM). Accumulations of synaptic vesicles in dilatations of axons suggest sites of neurotransmitter release. Note presence of external lamina, myofilaments, and dense bodies.

A8 Diagram illustrating connective tissue coats in skeletal muscle.

A9 Diagram of skeletal muscle fibers (cells) depicting banding pattern as seen by LM.

B1 LM of skeletal muscle, cross sectioned. Individual fibers can be seen, with peripherally placed, multiple nuclei. (H & E).

B2 LM of skeletal muscle, longitudinally sectioned. Individual fibers are striated. (H & E)

B3 Diagram of skeletal muscle fiber illustrating ultrastructural features: myofibrils, sarcomeres, T-tubules, and sarcoplasmic reticulum.

B4 TEM of skeletal muscle, longitudinally sectioned. Registration of striation (sarcomeres) is apparent, as are mitochondria positioned between myofibrils. Portions of three muscle fibers (cells) are visible. Note the peripherally placed nucleus.

B5 Diagram illustrating contractile mechanism of skeletal muscle sarcomeres.

B6 TEM of sarcomeres in mouse skeletal muscle. Because of the tangential plane of section, the network of sarcoplasmic reticulum surrounding the sarcomere can be easily seen.

B7 Relationship of densely stained sarcoplasmic reticulum in two adjacent sarcomeres as seen by TEM. T-tubules (T) and terminal cisternae (tc) of the sarcoplasmic reticulum can be seen at junction of A and I bands in mammalian skeletal muscle. Also visible are sarcotubules of the reticulum (st).

B8 SEM of skeletal muscle fiber revealing invaginations of sarcolemma as T-tubules. Reticular fibers form a loose network on the sarcolemma. See B3.

B9 High magnification of T-tubule invagination (arrows) on surface of skeletal muscle fiber as seen by SEM. Z, Z-line of sarcomere.

C1 LM of myotendinous junction showing striated skeletal muscle joining tendon (collagen stains blue). Collagen in endomysium blends with collagen in tendon. (azan stain)

C2 Myotendinous junction (TEM). Fibroblast (Fb), collagen (C), and sarcomeres can be seen. Note indentation of cell membrane to increase surface area and termination of sarcomere in modified Z-line on plasmalemma.

C3 Diagram of motor end plate (MEP).

C4 LM of nerve crossing skeletal muscle and dividing into terminal branches, each with motor end plate. (silver stain)

C5 SEM of motor end plate after removal of collagen and basal lamina. A bundle of nerves (N) can be seen ending in two motor end plates (E). Observe the branching of the terminal portion of the nerve fiber in the motor end plate where it is in apposition to the muscle cell. A Schwann cell (S) covers the motor end plate. A small blood capillary (C) and a pericyte (P) are also visible.

C6 SEM of mouse skeletal muscle cell showing site (left) where motor end plate occupied deep furrows (synaptic cleft) in cell surface. Striations of sarcomeres in myofibrils, nuclei of the muscle cell, and a satellite cell are also seen in this micrograph.

C7 TEM of part of motor end plate. The terminal is sheathed by a Schwann cell process (S at top) which intrudes fingers (S at lower right) between the terminal and the muscle cell. Synaptic vesicles cluster around specialized regions of the presynaptic membrane (*), which are subtended by a dense cytoplasmic material forming the bands that face the mouths of muscle cell folds. Postsynaptic muscle membrane at tops of folds also is underlaid by a dense material which may represent its active or receptive zone. Compare with C6 and C8.

C8 TEM of motor end plate in which cholinergic receptors have been localized using HRP-labeled alpha-bungarotoxin. Compare the normal morphology in Figure A with that in Figure B which is stained for alpha-bungarotoxin (cholinergic receptors). Dense staining representing the presence of cholinergic receptors is seen on the postsynaptic membrane at the top of, and partly down the sides of, the junctional folds of the muscle cell.

C9 Protoplasmic fracture face of neuromuscular junction viewed by FF from outside the nerve terminal, showing cytoplasmic leaflet of its split membrane. Ridges (large arrows) face folds (F) in surface of the muscle. Small dimples in surface of the terminal beside the ridges (small arrows) are thought to be loci where synaptic vesicles were fixed as they fused with the plasmalemma. Compare with C7. Shadow angle is from upper right.

D1 Cross section of cardiac muscle cells as seen by LM. Nuclei of muscle fibers, when in the plane of section, are centrally located in the cell. (H & E)

D2 TEM of cardiac muscle cell in cross section. Identify mitochondria and cross sections of sarcomeres. Compare with D1. Nc1, nucleus; Mt, mitochondria; Mf1, myofibril; Cap, capillary.

D3 Cardiac muscle in longitudinal section (LM). Many vessels can be seen between fibers. Nuclei are central, with lipofuscin pigment (gold-brown granules) at nuclear poles. (H & E)

D4 Cardiac muscle in longitudinal section (TEM). Sarcomere registration is less precise than in skeletal muscle. Mitochondria are prominent.

D5 Drawing of cardiac muscle. Note differences in T-tubule (at Z-lines) and in sarcoplasmic reticulum (dyads) from arrangement found in skeletal muscle.

D6 LM of cardiac muscle in longitudinal section showing branching and intercalated disks. (H & E)

D7 Cardiac muscle (TEM) with intercalated disk running from upper left to center to lower right in the field. ID, intercalated disk; F, muscle fibril; M, mitochondrion.

D8 Higher magnification of intercalated disk (TEM). Note regions corresponding to gap junctions and fascia adherens.

D9 Drawing of conducting system of heart, including sinoatrial node, atrioventricular node, atrioventricular bundle, and bundle branches.

E1 LM of modified cardiac muscle cells (lightly stained in upper half of field). These are Purkinje fibers, modified for conduction. (H & E)

E2 Visualization of Purkinje system by use of PAS stain and LM. The cells in the system are more darkly stained than other cardiac muscle cells because of their glycogen content. Compare with E1.

E3 LM of Purkinje system (PAS stain) at high magnification. Nuclei are seen as negative images.

E4 TEM of Purkinje fiber (longitudinal section) in monkey heart. Note paucity of myofibrils and their distribution.

E5 TEM of Purkinje fiber at higher magnification. Compare this specialized muscle cell with normal cardiac muscle cell at bottom of field. Large amounts of glycogen and few myofibrils are seen in the Purkinje cell.

E6 TEM of atrial cardiac muscle cell. Unmyelinated nerve containing synaptic vesicles is seen in endomysium between muscle cell and endothelial cell (left). Small dense granules are characteristic of atrial muscle cells.

E7 Drawing of variations in neuron morphology. Types of neurons are not drawn to scale.

E8 Drawing of peripheral nervous system.

E9 Cross section of mouse spinal cord at LM level, showing central canal, white and gray matter, and dorsal root ganglion (DRG). (H & E)

F1 Dorsal root ganglion of mouse spinal cord at higher magnification (LM). Satellite cells surround the neurons. (H & E)

F2 Dorsal root ganglion of mouse spinal cord at still higher magnification (LM). Lipofuscin pigment is visible in some DRG neurons. Satellite cells surround neurons. (H & E)

F3 LM of dorsal root ganglion viewed by dark field microscopy after uptake of horseradish peroxidase. Note abundant nerve processes (which appear white) and cell bodies (pink).

F4 Drawing of motor neuron in ventral horn of spinal cord, and extension of axon into peripheral nervous system, where it terminates in motor end plates in skeletal muscle.

F5 LM of lower motor neurons (LMN) of mouse spinal cord. These large basophilic cells are seen in ventral horns (gray matter) of the spinal cord. (H & E)

F6 High-magnification LM of lower motor neuron of mouse spinal cord. This neuron exhibits a large euchromatic nucleus with prominent nucleolus, and basophilic chromophil substance (RER) called Nissl bodies. An axon, devoid of Nissl substance, emerges from cell at left at axon hillock. Cells are embedded in neuropil. Nuclei of neuroglial cells are seen in neuropil. (H & E)

F7 LM of neuron in cerebral cortex. Use of silver impregnation reveals neuronal processes extending from perikaryon and numerous processes from other cells passing through vicinity of this neuron.

F8 TEM of neuron in central nervous system, with numerous profiles of rough endoplasmic reticulum (corresponds to Nissl substance at LM level) and many mitochondria. Plasmalemma of neuron (runs from mid-right to upper left) separates neuron cytosol from surrounding neuropil and synaptic endings. (For drawings of axosomatic and axodendritic endings, see Fiche 5, Frame B4.)

F9 LM of peripheral nerve surrounded by connective tissue (epineurium) and segmented by perineurium into fasicles. Individual fibers (axons) within nerve are ensheathed by endoneurium and are seen in both cross and longitudinal sections. (This typical appearance is often called a "snake-fence" configuration.) (H & E)

G1 LM of axons surrounded by myelin sheath. Schwann cell nuclei (left center) are large and vesicular, and found within endoneurium which surrounds individual axon cylinders. (H & E)

G2 LM of peripheral nerve in longitudinal section. Clear nodal cytoplasm helps distinguish two nodes of Ranvier (at center and lower left). Nuclei present may include those of fibroblasts, endothelial cells, and Schwann cells. (H & E)

G3 Whole mount of myelinated dorsal root ganglion in culture (LM). Observe length of internodal segments (black lines). Unmyelinated fibers and neuronal cell bodies appear gray.

G4 SEM of isolated myelinated fibers of sciatic nerve. In A (left) the endoneurial sheath (En) and a node of Ranvier (NR) are clearly evident. The segmented appearance of the nerve fiber (arrows) is due to a number of incisures (clefts of Schmidt-Lantermann) in the myelin sheath. B (right) is a SEM at higher magnification of a node of Ranvier (NR) showing terminal portions of two Schwann cells (*). A delicate sheath of reticular fibers, together with some collagen fibers (arrows), is the endoneurial sheath (En).

G5 TEM showing longitudinal section through a node of Ranvier. The myelin sheaths of adjoining Schwann cells show distended individual lamellae (arrow), each of which is closely apposed to the axon membrane. The node of Ranvier is covered by cytoplasmic processes of the Schwann cell. These processes are separated from connective tissue interstitium by an external lamina (B), collagenous material resembling basal lamina of epithelium.

G6 TEM of myelinated and unmyelinated nerve fibers in cultured dorsal root ganglion. Observe Schwann cell and its processes in both myelinated and unmyelinated fibers.

G7 LM of peripheral nerve stained with azan. The epineurium is a thick sheath of collagen which stains blue. Septa of perineurium extend into the nerve, and a faint staining for collagen is also seen in the endoneurium surrounding each axon.

G8 LM in which collagen in endoneurium is stained blue, and neurokeratin (protein remnant of Schwann cell and of myelin) appears as pink network around individual axon cylinders. (azan stain)

G9 TEM showing cross section through branch of facial nerve. In the center of the endoneurial sheath are four Schwann cells, two of which contain myelinated (A) axons and two unmyelinated axons. All are surrounded by a collagenous sheath and two layers of flattened connective tissue cells. These fibroblasts are unique in that they are covered with an external lamina (B). Thus, this cellular perineurial sheath may function as a diffusion barrier to nutrients diffusing from capillaries to Schwann cells and nerve fibers within the sheath. SC, Schwann cell; N, nucleus; *, junctional area.

Acknowledgments

A4 Courtesy of Dr. David G. Chase, Cell Biology Research Laboratory, Veteran's Administration Hospital, Sepulveda, CA.

A6 Courtesy of Dr. Frederic S. Fay, Department of Physiology, University of Massachusetts, Worchester, MA.

B4 Courtesy of Dr. J. H. Venable, Department of Anatomy, Colorado State University, Fort Collins, CO.

B5 Reproduced with permission from C. P. Leblond, *Histology*, 8th edition, A. W. Ham and D. H. Cormack, editors, Lippincott, Philadelphia, PA, 1979.

B6 Courtesy of Ms. Barbara Zweber, Department of Physical Medicine and Rehabilitation, University of Minnesota, Minneapolis, MN.

B7 Reproduced with permission from M. S. Forbes, Journal of Ultrastructural Research 60:306, 1977.

B8, B9 Reproduced with permission from Lawrence P. McCallister and Robert Hadek, Journal of Ultrastructural Research 33:360, 1977. Special thanks expressed to Evjes Equipment Co., Chicago, IL, for technical assistance.

C2 Reproduced with permission from David Smith, *Muscle*, Academic Press, New York, NY, 1972.

C4 Courtesy of Dr. Paul C. Letourneau, Department of Anatomy, Medical School, University of Minnesota, Minneapolis, MN.

C5 Reproduced with permission from Tsuneo Fujita, *SEM Atlas of Cells and Tissues*, T. Fujita, K. Tanaka, and J. Tokunaga, editors, Igaku-Shoin, Tokyo, Japan, 1981.

C6 Courtesy of Drs. Rosemary Mazanet and Clara Franzini-Armstrong, Department of Biology, University of Pennsylvania, Philadelphia, PA.

C7, C9 Courtesy of Dr. J. E. Heuser, Department of Physiology and Biophysics, Washington University, St. Louis, MO.

C8 Reproduced with permission from Steven J. Burden, Journal of Cell Biology 82:412-25, August 1979.

D2 Reproduced with permission from S. McNutt and D. W. Fawcett, Journal of Cell Biology 42:1, 1969.

D4, D7, D8, E6 Courtesy of Dr. David G. Chase, Cell Biology Research Laboratory, Veteran's Administration Hospital, Sepulveda, CA.

D5 Reproduced with permission from *Gray's Anatomy*, 35th British edition, R. Warwick and P. L. Williams, Longman, Edinburgh, Scotland, 1973.

E4 Reproduced with permission from S. Viragh, *Ultrastructure of the Mammalian Heart*, C. E. Challice and S. Viragh, editors, Academic Press, Orlando, FL, 1973.

E5 Courtesy of Dr. S. Viragh, Department of Pathology, Postgraduate Medical School, Budapest, Hungary.

F3 Courtesy of Dr. Glenn Giesler, Department of Anatomy, Medical School, University of Minnesota, Minneapolis, MN.

F8 Reproduced with permission from Michael J. Cullen, Tissue and Cell 9(1):1-10, 1977.

G3 Courtesy of Drs. R. D. Bunge and M. B. Bunge, Department of Anatomy, Washington University School of Medicine, St. Louis, MO.

G4 Reproduced with permission from Pietro M. Motta, Atlante di microscopia elettronica a scansione, Piccin Nuova Libraria S.p.A., Padova, Italy.

G5, G9 Reproduced with permission from Jean Babel, A. Bischoff, and H. Spoendlin, *Ultrastructure of the Peripheral Nervous System and Sense Organs*, A. Bischoff, editor, Georg Thieme Verlag, Stuttgart, Germany, 1970.

G6 Courtesy of Drs. Mary B. Bunge and David S. Copio, Department of Anatomy, Washington University School of Medicine, St. Louis, MO.

A1 Drawing of autonomic nervous system, with sympathetic and parasympathetic divisions.

A2 Cross section (TEM) of rat abdominal vagus nerve, showing myelinated (ma) and unmyelinated fibers, two Schwann cells (Sc), and external lamina (arrows). Small, dense, circular profiles are cross sections of reticular fibers in endoneurium.

A3 TEM of unmyelinated nerve in connective tissue. Axons are enfolded in Schwann cell cytoplasm, and some contain synaptic vesicles. Note the presence of external lamina on Schwann cell.

A4 LM of autonomic ganglion in Auerbach's plexus in esophagus. Cell bodies (center) are large, basophilic, postganglionic neurons of parasympathetic nervous system. See A1. (H & E)

A5 Higher-magnification LM of Auerbach's plexus seen in A4. Basophilic neurons are surrounded by satellite cells. (H & E)

A6 Low-power LM of myenteric plexus in whole mount of small intestine, showing distribution of nerve cell bodies and fibers stained for 5-Hydroxytryptamine immunoreactivity. Double arrows indicate direction of longitudinal muscle. Immunoreactivity is seen in fibers of internodal strands (is). Some nerve cell bodies can be seen (single arrows) within ganglia of the plexus (g).

A7 TEM of parasympathetic neuronal cell bodies in myenteric plexus. Observe "glial-like" satellite or capsule cells surrounding neuronal cell bodies. cm, circular muscle; lm, longitudinal muscle; n, neuron; g, capsule or satellite cells; c, connective tissue.

A8 LM of parasympathetic neuron in epicardium of heart. (H & E)

A9 TEM of parasympathetic nerve cell body in mouse epicardium. Note eccentric nucleus.

B1 LM of parasympathetic (postganglionic) cell body and adjacent satellite cell within pancreas. (H & E)

B2 LM of Meissner's corpuscle (center) in skin, where it is a touch receptor in papillary layer of dermis. (H & E)

B3 LM of Pacinian corpuscle. It is a pressure receptor distributed throughout dermis and subcutaneous tissue, and in joint capsules, mesenteries, urinary bladder, and other tissues that may be deformed by pressure. (H & E)

B4 Diagram of synapses and their classification.

B5 TEM of synapses (arrows indicate direction of transmission) between terminal boutons and a dendrite (D). Note differences in shape of vesicles. Round vesicles are thought to contain excitatory neurotransmitters; flattened vesicles, inhibitory neurotransmitters. My, myelin.

B6 TEM of synaptic terminals showing pre- and postsynaptic thickening of plasmalemma. Note mitochondria and synaptic vesicles. The synaptic terminal (right) contains round vesicles with excitatory neurotransmitters and dense-cored vesicles that contain adrenergic-peptidergic neurotransmitters. The arrow (in left picture) points to postsynaptic membrane thickening.

B7-B9 Blank

C1 Drawing of bone marrow circulation.

C2 Macrophotograph of bone marrow showing cartilage (top), bone spicules, and marrow spaces.

C3 Longitudinal section of bone depicting epiphyseal plate (top), spicules of forming bone, and marrow. LM, low magnification. Compare with C2. (H & E)

C4 LM of section of bone marrow showing hemopoietic compartment and sinusoids of bone marrow as revealed by presence of red blood cells. (H & E)

C5 SEM of bone marrow. Sinusoids open into lumen of vessel (right). Cells of hemopoietic compartment can be seen between sinusoids.

C6 LM of hemopoietic cells and sinusoids of bone marrow. Note vascular wall of sinusoid (center) and different types of hemopoietic cells, including developing eosinophils.

C7 TEM of hemopoietic cells of bone marrow adjoining a sinusoid (right) lined by endothelial cells.

C8 Drawing of pluripotent stem cell and its differentiation into hemopoietic cell lines.

C9 TEM of hemopoietic stem cell revealing large nucleus and prominent nucleolus. This cell, resembling a large lymphocyte, contains many free ribosomes, some rough endoplasmic reticulum (er), and mitochondria (m) in the cytoplasm.

D1 Diagram of erythrocytic series, with keys to identification.

D2 LM of pronormoblast with large, smooth nucleus and nucleoli. The nuclear membrane is distinct and the cytoplasm relatively basophilic. Also seen are three granulocytes, two late polychromatophilic normoblasts, and numerous mature red blood cells. (Wright's stain)

D3 TEM of pronormoblast. Notice prominent nucleolus, and free ribosomes in cytoplasm which account for the basophilia at LM level.

D4 LM comparison of pronormoblast (upper right) and basophilic normoblast (lower left). In the latter cell, the nuclear chromatin is more condensed and the cytoplasm is navy blue, making this the most basophilic cell in bone marrow. (Wright's stain)

D5 LM comparison of basophilic normoblast (lower center) and plasma cell (upper right). The latter cell contains more cytoplasm. Note also that unlike the basophilic normoblast, the plasma cell nucleus is eccentric and a Hof area (Golgi apparatus) is apparent. A mature neutrophil is at center. (Wright's stain)

D6 TEM of basophilic normoblast (upper left) with numerous ribosomes, and two polychromatophilic normoblasts which are smaller, with more condensed nuclear chromatin. Parts of granular leukocytes are also visible (lower left and upper right).

D7 LM of group of polychromatophilic normoblasts, showing variation in size and in cytoplasmic staining. The larger polychromatophilic normoblasts are less mature than the smaller ones, which exhibit very dense, pyknotic nuclei. Several polychromatophilic red blood cells with bluish-staining cytoplasm of various shades can be seen. Note the normoblast that is about to extrude its nucleus (just left of center). (Wright's stain)

D8 TEM of polychromatophilic normoblast. Observe condensed nuclear chromatin and relatively abundant ribosomes in the cytoplasm.

D9 LM of polychromatophilic normoblast in mitosis (center) surrounded by developing neutrophils. (Wright's stain)

E1 Normoblasts as seen by TEM in two stages of nuclear extrusion. Note that a thin rim of cytoplasm is carried away with the nucleus.

E2 LM of orthochromatophilic normoblast. The cytoplasm is the same color as mature red blood cells, and the nucleus is extremely small and dense (pyknotic). Granulocytes in various stages of maturation are also visible (bottom). (Wright's stain)

E3 TEM of bone marrow sinusoid (S at upper right) and adjacent cells. An erythrocyte (E) is extruding its nucleus (lower center). Above and to its left are seen a reticulocyte (polychromatophilic red blood cell, indicated by R) and a polychromatophilic normoblast. A mature neutrophil (N) is entering the sinusoid by diapedesis. B, basophil; Meg, megakaryocyte.

E4 TEM of macrophage that has ingested extruded normoblast nuclei (center). Parts of two polychromatophilic normoblasts are visible (left).

E5 Two red blood cells on fibrin clot as seen by SEM. Note difference in size. Does this correlate with cell age?

E6 Diagram of granulocytic series, with keys to identification.

E7 Myeloblast (large cell to right of center) as seen by LM. This cell has a very big vesicular nucleus, indistinct nuclear membrane, and scattered cytoplasmic azure granulation. (Wright's stain)

E8 Promyelocyte (large cell at lower right) as seen by LM. It has a larger proportion of cytoplasm as compared with the myeloblast (or later stages). Many large azurophilic granules are present in the cytoplasm. The nuclear membrane is distinct. Compare with E7. Observe the N. myelocyte (left) and the N. metamyelocyte (above). (Wright's stain)

E9 TEM of promyelocyte (left center). The cytoplasm is filled with large electron-dense granules which appear as azurophilic granules by LM.

F1 LM comparison of large promyelocyte (upper left) with succeeding stages of neutrophilic maturation. Observe the N. myelocyte next to it on either side (upper center, lower left), the N. metamyelocyte with slightly indented nucleus (far right), and the band form neutrophil (below and to the right of the promyelocyte). (Wright's stain)

F2 LM showing neutrophilic myelocyte (upper center) and two neutrophilic myelocytes (directly below) in mitosis. To the right are two lymphocytes. (Wright's stain)

F3 TEM of neutrophilic myelocyte. Note the specific granules (s) present in this cell are variable in size, shape, and density. Some azurophilic, or primary (P), granules are also seen.

F4 LM of neutrophilic myelocyte seen in company with several N. metamyelocytes (indented nuclei), two band forms, and two almost mature neutrophils. (Wright's stain)

F5 TEM of neutrophilic metamyelocyte with deeply indented nucleus. n, nucleus; ch, chromatin; Gc, Golgi complex; er, rough endoplasmic reticulum; m, mitochondria; ag, azure granule; ig, immature granule; sg, specific granule.

F6 LM of promyelocyte (largest cell) with neutrophilic myelocyte above it, neutrophilic band form above and to its right, and three mature neutrophils. Identify the deeply basophilic cell to the right of center. (Wright's stain)

F7 TEM of mature neutrophil exhibiting lobulated nucleus (N). Lobules are connected by strands of nucleoplasm which are out of the plane of the section. Note that organelles and secretory granules are clearly visible. G, Golgi; c, centriole; m, mitochondria.

F8 LM of eosinophilic myelocyte. Identify other cells in field. (Wright's stain)

F9 LM of eosinophilic myelocyte, metamyelocyte, and (typically) bilobed mature eosinophil. Early eosinophil myelocytes may have slightly basophilic cytoplasm and specific granules. Can you identify cells at left of field? (Wright's stain)

G1 LM of bone marrow cells, including a number of developing granulocytes, a polychromatophilic normoblast in mitosis, and two mature neutrophils. (Wright's stain). Identify the early-stage granulocytes.

G2 LM of developing basophil (upper left) and two band form neutrophils (upper right). What other cell types are present? (Wright's stain)

G3 Diagram showing maturation of red and white cell lines and total number of cells found in bone marrow and in peripheral blood compartments.

G4 LM of plasma cell in bone marrow. Identify other cell types in the field. (Wright's stain)

G5 LM of osteoclast in bone marrow. Can you recognize other marrow cell types? (Wright's stain)

G6 LM of promegakaryocyte in bone marrow. (Wright's stain)

G7 LM of megakaryocyte in bone marrow. Note the large, twisted, lobulated nucleus of this polyploid cell. Platelets stream from the cytoplasm of these cells into the sinusoids of the bone marrow. (Wright's stain)

G8 TEM of megakaryocyte. Note the large polymorphic nucleus. The cytoplasm contains granules of various density. The extensive SER (platelet demarcation membranes) divides the cytoplasm into developing platelets which are finely granular and contain packets of microfilaments but are largely free of organelles.

G9 TEM of circulating platelet in capillary of lamina propria of intestine.

Acknowledgments

A2, A7 Reproduced with permission from Giorgio Gabella, *Structure of the Autonomic Nervous System*, Chapman and Hall, London, England, 1976.

A6 Reproduced with permission from M. Costa, J. B. Furness, A. C. Cuello, A. A. J. Verhofstad, H. W. J. Steinbusch, and R. P. Elde, Neuroscience, Vol. 7, No. 2, February 1982.

A9 Courtesy of Dr. A. Yamauchi, Department of Anatomy, Iwate Medical University, Morioka, Japan.

B5 Reproduced with permission from Koji Uchizono, *Excitation and Inhibition, Synaptic Morphology*, Igaku-Shoin, Tokyo, Japan, 1975.

B6 Reproduced with permission from Sanford Palay and Victoria Chan-Palay, *Handbook of Physiology*, Section 1, Vol. 1, The American Physiological Society, Bethesda, MD, 1977.

C2 Reproduced with permission from Lennart Nilsson, *Behold Man*, Little, Brown, Boston, MA, 1973.

C5 Courtesy of Drs. L. Weiss, Department of Animal Biology, University of Pennsylvania, Philadelphia, PA, and L. T. Chen, Department of Anatomy, University of South Florida, Tampa, FL.

C7 Courtesy of Drs. L. T. Chen, Department of Anatomy, University of South Florida, Tampa, FL, and L. Weiss, Department of Animal Biology, University of Pennsylvania, Philadelphia, PA.

C9, F5 Reproduced with permission from Dorothy Bainton, Developmental Biology 44:223-27, 1975.

D3, D8, E1, E4 Courtesy of Dr. Kenneth Campbell, Department of Pathology, Reproductive Biology Program, University of Michigan, Ann Arbor, MI.

D6, E9, G8 Courtesy of Dr. G. Adolph Ackerman, Department of Anatomy, Ohio State University, Columbus, OH.

E3 Reproduced with permission from L. T. Chen, Blood 39:102, 1972.

F3, F7 Reproduced with permission from J. C. Cawley and F. G. J. Hayhoe, *Ultrastructure of Haemic Cells*, Saunders, London, England, 1973.

Index

Following is a key to abbreviations used in the index:

D	diagram	SEM	scanning electron micrograph
FF	freeze fracture	T	table
LM	light micrograph	TEM	transmission electron micrograph
M	macrophotograph		

Boldface capital F precedes fiche number

This page intentionally left blank

Stanley L. Erlandsen earned his doctorate in anatomy at the University of Minnesota in 1967, and was a postdoctoral fellow at the University of Washington. He has taught at the University of Iowa and, since 1974, in the Medical School at the University of Minnesota, where he is now professor of anatomy. Erlandsen is co-author of *Giardia and Giardiasis: Biology, Pathogenesis and Epidemiology* (1984) and serves on the editorial boards of *The Journal of Histochemistry and Cytochemistry* and *The Anatomical Record*.

Jean E. Magney earned a B.S. in occupational therapy and an M.S. in anatomy at the University of Minnesota. She was an instructor and illustrator in the department of physical medicine and rehabilitation at Minnesota from 1971 until 1980, and since 1979 has been an instructor in the department of anatomy, University of Minnesota Medical School. Magney is co-author and illustrator of *Care of the Disabled Urinary Tract* (now in press).